Time scale controversy: Accurate orbital calibration of the early Paleogene

Thomas Westerhold, Ursula Röhl, Jacques Laskar

Geochemistry Geophysics Geosystems G3

Article
Volume 13, Number 6
23 June 2012
Q06015, doi:10.1029/2012GC004096
ISSN: 1525-2027

Published by AGU and the Geochemical Society

Time scale controversy: Accurate orbital calibration of the early Paleogene

Thomas Westerhold and Ursula Röhl

MARUM–Center for Marine Environmental Sciences, University of Bremen, Leobener Strasse, DE-28359 Bremen, Germany (twesterhold@marum.de; uroehl@marum.de)

Jacques Laskar

Astronomie et Systèmes Dynamiques, IMCCE-CNRS UMR8028, Observatoire de Paris, UPMC, 77 Avenue Denfert-Rochereau, FR-75014 Paris, France (jacques.laskar@imcce.fr)

[1] Timing is crucial to understanding the causes and consequences of events in Earth history. The calibration of geological time relies heavily on the accuracy of radioisotopic and astronomical dating. Uncertainties in the computations of Earth's orbital parameters and in radioisotopic dating have hampered the construction of a reliable astronomically calibrated time scale beyond 40 Ma. Attempts to construct a robust astronomically tuned time scale for the early Paleogene by integrating radioisotopic and astronomical dating are only partially consistent. Here, using the new La2010 and La2011 orbital solutions, we present the first accurate astronomically calibrated time scale for the early Paleogene (47–65 Ma) uniquely based on astronomical tuning and thus independent of the radioisotopic determination of the Fish Canyon standard. Comparison with geological data confirms the stability of the new La2011 solution back to ~54 Ma. Subsequent anchoring of floating chronologies to the La2011 solution using the very long eccentricity nodes provides an absolute age of 55.530 ± 0.05 Ma for the onset of the Paleocene/Eocene Thermal Maximum (PETM), 54.850 ± 0.05 Ma for the early Eocene ash −17, and 65.250 ± 0.06 Ma for the K/Pg boundary. The new astrochronology presented here indicates that the intercalibration and synchronization of U/Pb and $^{40}Ar/^{39}Ar$ radioisotopic geochronology is much more challenging than previously thought.

Components: 10,500 words, 8 figures, 3 tables.

Keywords: PETM; astronomical calibration of the Paleogene; radioisotopic dating.

Index Terms: 1115 Geochronology: Radioisotope geochronology; 1165 Geochronology: Sedimentary geochronology; 9606 Information Related to Geologic Time: Paleogene.

Received 9 February 2012; **Revised** 4 May 2012; **Accepted** 16 May 2012; **Published** 23 June 2012.

Westerhold, T., U. Röhl, and J. Laskar (2012), Time scale controversy: Accurate orbital calibration of the early Paleogene, *Geochem. Geophys. Geosyst.*, *13*, Q06015, doi:10.1029/2012GC004096.

1. Introduction

[2] Temporal relations are the key to causality arguments in Earth's history [*Renne et al.*, 1998; *Min et al.*, 2000; *Kuiper et al.*, 2008; *Renne et al.*, 2010]. Our understanding of global change mechanisms and the dynamics of a rapidly changing climate system depends upon a precise knowledge of the dates as well as the rates of change in the geological past. An accurate timescale is the backbone for reconstructing Earth's history in order

to identify mechanisms associated with past prominent global events like the Paleocene/Eocene Thermal Maximum (PETM) more than 55 myr ago. As a numerical dating method, astronomical tuning, the correlation of cyclic variations in the geological record to astronomical computations of the insolation quantities on Earth, has revolutionized the age calibration of the geological time scale [*Shackleton et al.*, 1990; *Lourens et al.*, 2004; *Hilgen*, 2010]. An astronomically tuned geological time scale is now available for the last 40 million years [*Lourens et al.*, 2004; *Pälike et al.*, 2006b]. Efforts to extend the astronomically calibrated time scale into the early Paleogene have been hampered by fundamental problems related to the early to-late Eocene "cyclostratigraphic gap," an interval in the middle Paleogene that has not yet been completely covered by cyclostratigraphic studies in pelagic sediments [*Pälike and Hilgen*, 2008], by the uncertainties and limits of astronomical calculations [*Laskar et al.*, 2004, 2011b], and by uncertainties in radioisotopic age constraints [*Machlus et al.*, 2004; *Westerhold and Röhl*, 2009].

[3] Due to the chaotic motion of planets in the inner Solar System, the validity of the orbital solutions with increasing age is limited. Using the La2004 [*Laskar et al.*, 2004] solution, an accurate age determination of successive minima in the very long eccentricity cycle (~2.4 myr) used as first-order tie points for orbitally tuned time scales [*Lourens et al.*, 2004; *Pälike et al.*, 2004] is not possible for time series older than 40 Ma. Beyond 40 Ma, tuning for the long eccentricity cycle (405-kyr) is feasible because of its stability far back in time [*Laskar et al.*, 2004]. Floating cyclostratigraphic frameworks for the Paleocene and earliest Eocene [*Dinarès-Turell et al.*, 2003; *Lourens et al.*, 2005; *Westerhold et al.*, 2008; *Westerhold and Röhl*, 2009] (65 to 52 Ma), as well as the Cretaceous [*Sprovieri et al.*, 2006; *Husson et al.*, 2011] are therefore based on the recognition of the 405-kyr cycle. To obtain accurate numerical ages, anchoring of these floating time scales via highly precise, recalibrated absolute radioisotopic dates of ash layers was proposed [*Renne et al.*, 1994; *Hilgen et al.*, 1997; *Kuiper et al.*, 2008]. The accuracy of the widely used $^{40}Ar/^{39}Ar$ radioisotopic dating method mainly depends on the accurate age of the dating standards and exact knowledge of the radioactive decay constants [*Min et al.*, 2000]. Intercalibration between high-precision radioisotopic dating and astronomical tuning in Neogene geological successions [*Kuiper et al.*, 2008] resulted in the recalibration of the Fish Canyon sanidine (FC) standard age, eliminating discrepancies between $^{40}Ar/^{39}Ar$ and U/Pb radioisotopic ages [*Schoene and Bowring*, 2006]. But this synchronization of dating tools was challenged recently by the observation of a discrepancy between astronomical and $^{40}Ar/^{39}Ar$ age estimates for the Matuyama-Brunhes (M-B) boundary [*Channell et al.*, 2010]. Similar possible inconsistencies between astronomical and radioisotopic dates based on the *Kuiper et al.* [2008] FC calibration have been observed in Paleocene to early Eocene deep-sea successions [*Westerhold et al.*, 2007, 2008; *Westerhold and Röhl*, 2009; *Westerhold et al.*, 2009] leading to an up to now unsolved dating dilemma [*Hilgen et al.*, 2010; *Westerhold et al.*, 2009].

[4] Here we try to solve the dating dilemma by comparing the expression of the very long eccentricity-cycle minima in new orbital solutions for eccentricity (La2010 [*Laskar et al.*, 2011a] and La2011 [*Laskar et al.*, 2011b]) with geological data (Figure 1) that contain eccentricity-modulated precession cycles.

2. La2010 and La2011 Orbital Solutions for Eccentricity

[5] At present, the most advanced Earth orbital and rotational solution has been obtained by a direct numerical integration of the planet orbits and the precession of the Earth spin axis – the La2004 solution. This solution has been used for the astronomical calibration of the Neogene [*Lourens et al.*, 2004] in the GTS2004 geological time scale [*Gradstein et al.*, 2004]. The time of validity of this solution is estimated to be at ~40 Ma. Extending the astronomically calibrated geological time scale into the Paleogene is hampered by the limited accuracy of available orbital solution in times older than 40 Ma [*Laskar et al.*, 2004; *Machlus et al.*, 2004] (Figure 2a). Nevertheless building an orbitally calibrated stratigraphic framework based on the identification of the stable long eccentricity cycle (405-kyr) is still possible [*Laskar et al.*, 2004] for older periods. Although in the absence of long continuous records it results in floating time scales only.

[6] At present, there is a large international effort toward the construction of a complete astronomically calibrated geological time scale over the full Cenozoic era (GTSnext; http://www.gtsnext.eu). This will require the accomplishment of an orbital solution for the Earth motion back to 65 Ma. But this is not an easy task, as due to the chaotic motion of the system [*Laskar*, 1990, 1999], the initial uncertainty is

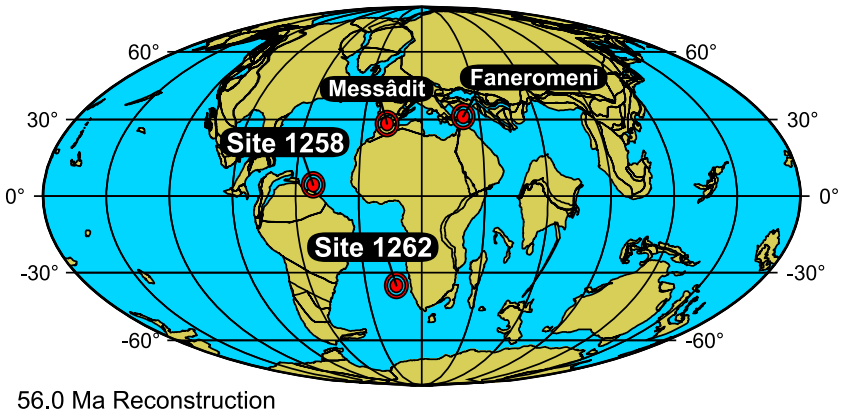

Figure 1. Map showing the location of ODP Sites 1262 [*Zachos et al.*, 2004] and 1258 [*Erbacher et al.*, 2004] as well as position of the Faneromeni [*Krijgsman et al.*, 1994] and Messâdit [*Roger et al.*, 2000] sections plotted in the 55 Ma paleogeographic reconstruction (http://www.odsn.de [*Hay et al.*, 1999]).

multiplied by 10 every 10 myr. Extending the La2004 solution from 40 to 65 Ma is thus equivalent to an improvement of the full gravitational model of more than 2 orders of magnitude. In order to improve the long-term ephemerides, the group of the Institut de Mécanique Céleste et de Calcul des Éphémérides (IMCCE) at Paris Observatory developed a new high precision planetary ephemeris called INPOP [*Fienga et al.*, 2008, 2009, 2011] (Intégration Numérique Planétaire de l'Observatoire de Paris). This precise model is adjusted to all available terrestrial and space mission tracking observations. An innovative feature of the INPOP ephemerides compared to the available equivalent solutions from JPL/NASA, is the capacity to be extended on long time, as much as 1 myr, which is then used as reference for the construction of the long-term planetary ephemerides La2010 [*Laskar et al.*, 2011a] that provide a reliable evolution of the Earth orbit over 50 Ma. In fact, in order to evaluate the uncertainty of the long-term solution, several solutions were computed corresponding to various settings: La2010a, b, c were adjusted to the INPOP08 ephemeris [*Fienga et al.*, 2009], while La2010d was adjusted to the previous model INPOP06 [*Fienga et al.*, 2008].

[7] More recently, using an increased set of observations, the new high precision INPOP10a ephemeris was released [*Fienga et al.*, 2011]. This allowed the construction of a new long-term solution La2011 [*Laskar et al.*, 2011b] which benefited also from improvements in the numerical algorithm for the computation of the solution. As a result, the integration time in La2011 was decreased while the numerical accuracy was increased [*Laskar et al.*, 2011b]. The solution La2011 was constructed together with clones of the solution (La2011m2, La2011p2, La2011m4) with changes in the initial position of the minor planets of respectively −15 m, +15 m, and −1.5 mm, much less than the present determination of their position which amounts to several hundreds of km. Moreover, the same study [*Laskar et al.*, 2011b] demonstrated that the motion of Ceres and Vesta, is highly chaotic. As a consequence, a precise calculation of Earth's eccentricity beyond 60 Ma is not, and probably will never be, possible [*Laskar et al.*, 2011b]. This makes direct tuning of geological data to the short eccentricity curve (100-kyr) impossible for interval older than 60 Ma and demonstrates that an astronomically tuned framework beyond 60 Ma can only be based

Figure 2. Eccentricity as well as the long (405-kyr) and the very-long (2.4-myr) eccentricity cycle of the La2004 [*Laskar et al.*, 2004], La2010 [*Laskar et al.*, 2011a] and La2011 [*Laskar et al.*, 2011b] solutions from 40 to 60 Ma. The amplitude modulations have been extracted with the program ENVELOPE [*Schulz et al.*, 1999]. (a) Eccentricity of five La2004 solutions (J. Laskar, unpublished data) to test the stability of the nominal solution. The plot illustrates the fact that prior to ∼40 Ma the error in the La2004 solution increases and thus prevents a direct calibration of geological time series. (b) Eccentricity of the La2010 solution. The plot shows that the amplitude modulation of the La2010 eccentricity solution is getting unstable beyond 50 Ma. (c) Eccentricity of the La2011 solutions. The plot illustrates that the La2011 solution is not reliable beyond ∼60 Ma. (d) Eccentricity of the La2010a, La2010d and La2011 solutions. The plot demonstrates on the one hand that the position of the very-long eccentricity minima of La2010d and La2011coincide perfectly up to about 54 Ma and on the other hand that all three short eccentricity solutions are very similar, with exception of the very long eccentricity minima, up to 50 Ma.

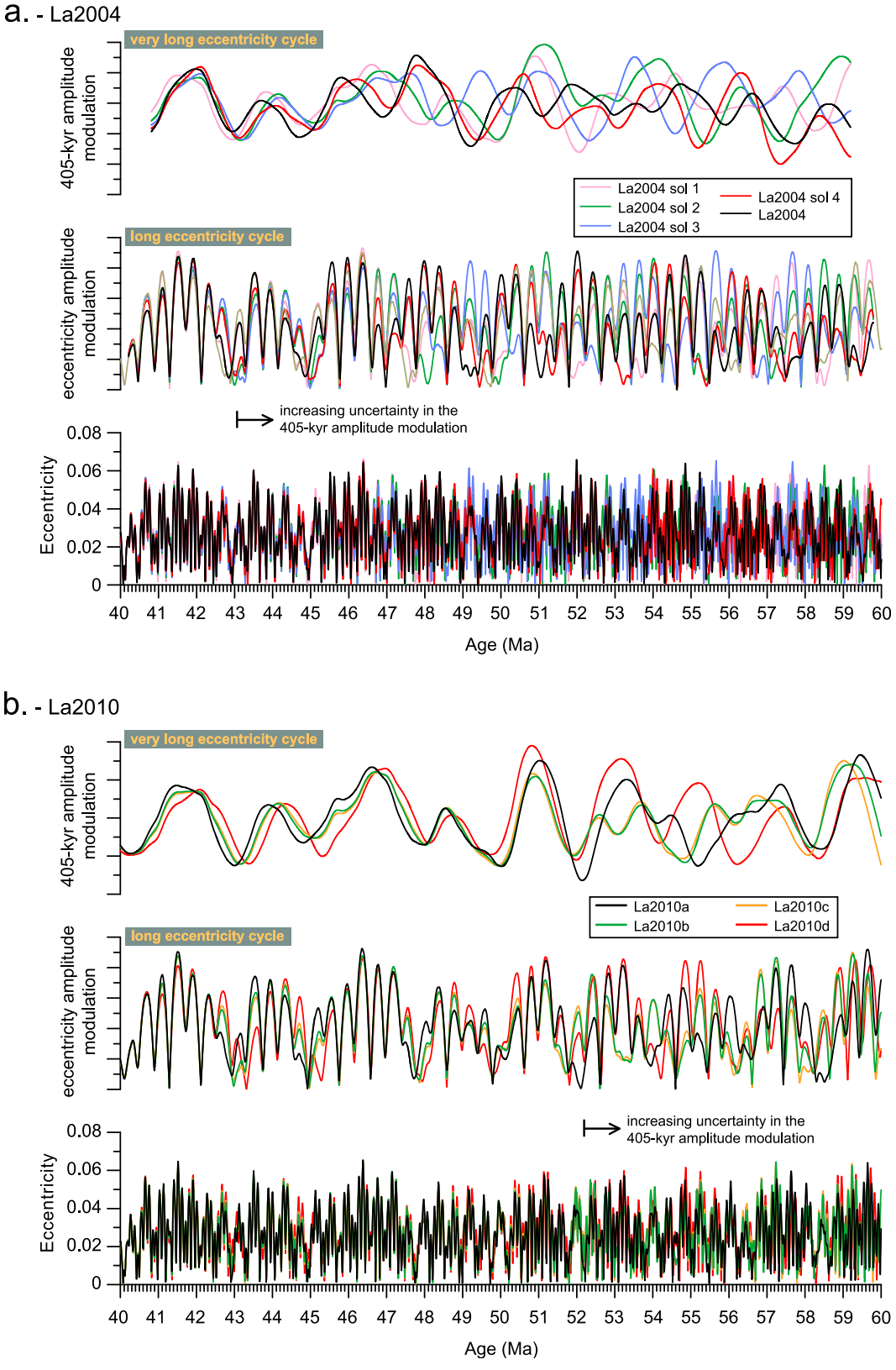
a. - La2004
very long eccentricity cycle
405-kyr amplitude modulation
La2004 sol 1
La2004 sol 2
La2004 sol 3
La2004 sol 4
La2004
long eccentricity cycle
eccentricity amplitude modulation
increasing uncertainty in the 405-kyr amplitude modulation
Eccentricity
0.08
0.06
0.04
0.02
0
40 41 42 43 44 45 46 47 48 49 50 51 52 53 54 55 56 57 58 59 60
Age (Ma)
b. - La2010
very long eccentricity cycle
405-kyr amplitude modulation
La2010a
La2010b
La2010c
La2010d
long eccentricity cycle
eccentricity amplitude modulation
increasing uncertainty in the 405-kyr amplitude modulation
Eccentricity
0.08
0.06
0.04
0.02
0
40 41 42 43 44 45 46 47 48 49 50 51 52 53 54 55 56 57 58 59 60
Age (Ma)

Figure 2

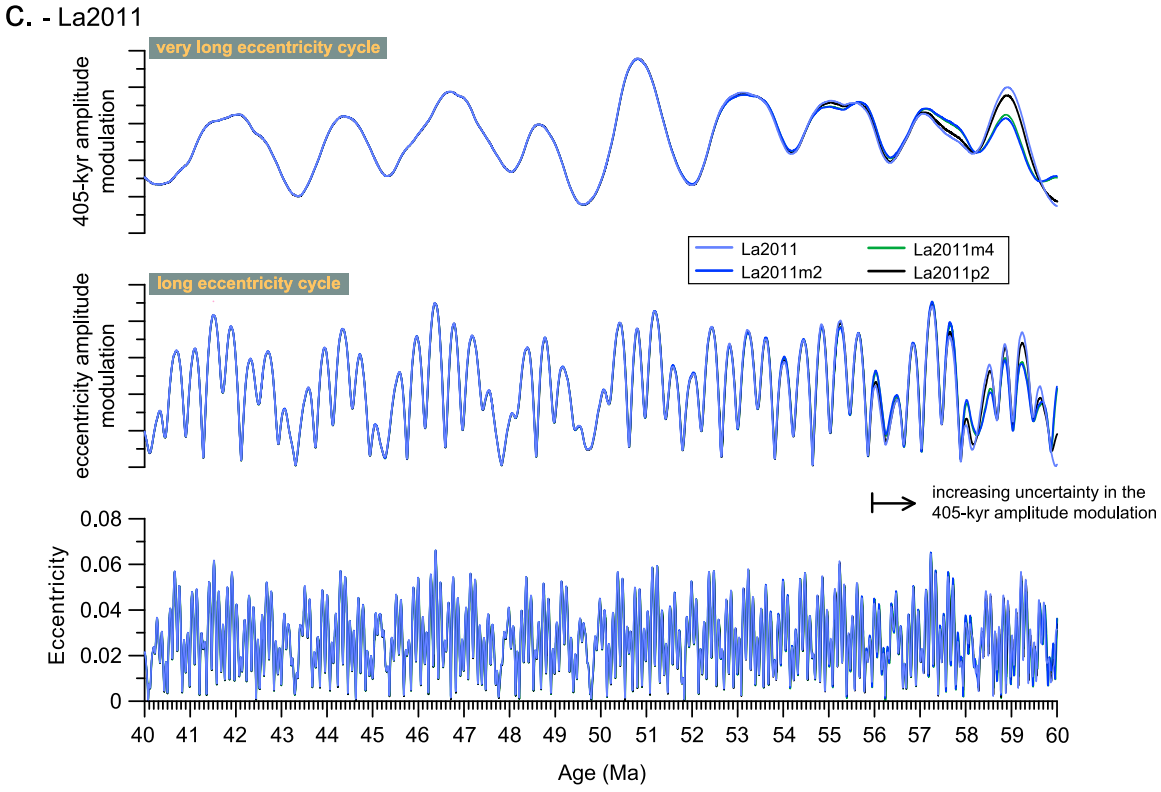

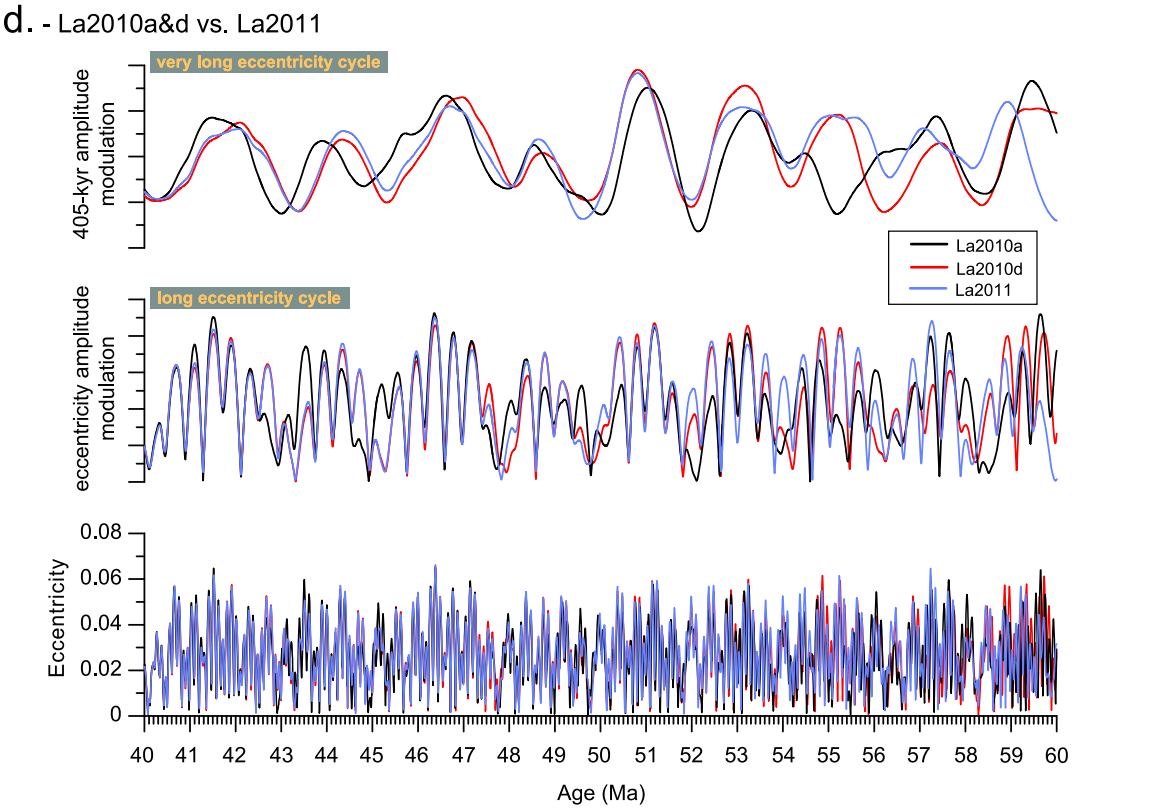

Figure 2. (continued)

on the identification of the stable long eccentricity cycle (405-kyr) [*Laskar et al.*, 2004].

[8] On the opposite, before 50 Ma, the solution La2010 and even better, La2011 can be used for a fine tuning to the eccentricity curve. The interval 50 Ma to 60 Ma remains in question, as it is difficult at present to assert the validity of the orbital solutions La2010 and La2011 in this range at the short eccentricity level.

[9] In order to test the stability of the La2010 and La2011 nominal solutions with respect to the very long eccentricity modulation (~2.4 myr), other solutions with slightly different settings have been computed and compared. The extraction of the amplitude modulation of the four different eccentricity solutions in La2010 suggests that this solution is not reliable beyond 52 Ma (Figure 2b). In the same way, the amplitude modulation of four different eccentricity solutions in the new La2011 shows that the solution cannot be trusted after 60 Ma (Figure 2c), but this upper bound does not provide information on how far these solutions can be trusted, as the different La2011 solutions are very small variations around the same solution. On the opposite, comparing the amplitude modulation between La2010a, La2010d and La2011 (Figure 2d) shows that the La2010d solution is similar to La2011 up to 54 Ma. This is a very strong indication that the La2010d and even better the La2011 solution is valid over 54 Ma. Indeed, La2010d is based on the INPOP06 ephemeris [*Fienga et al.*, 2008], while La2010a, b, c are based on INPOP08 [*Fienga et al.*, 2009]. The construction of INPOP10a [*Fienga et al.*, 2011] has now demonstrated that the long-term behavior of INPOP08 [*Fienga et al.*, 2009] is not as good as the one of INPOP06 [*Fienga et al.*, 2008], which is closer to INPOP10a [*Fienga et al.*, 2011] which is used as a reference for La2011. Comparison of the two independent solutions La2010d and La2011 is thus a good way to evaluate the time of validity of these solutions, which can be set to 54 Ma. At least the amplitude modulation of eccentricity is stable back to 54 Ma for the La2011 solution as can be concluded from the comparison between geological data and the La2010a, La2010d and La2011 solutions (see Discussion).

3. Geological Data

[10] The geological data we use are iron (Fe) intensity data based on X-ray fluorescence (XRF) core-scanning measurements of marine sediments drilled at Ocean Drilling Program (ODP) Sites 1258 [*Westerhold and Röhl*, 2009] (Leg 207; Demerara Rise) and 1262 [*Westerhold et al.*, 2007, 2008] (Leg 208; Walvis Ridge), located in the Atlantic Ocean (Figure 1). Both records have a robust cyclostratigraphic framework based on the stable 405-kyr cycle from 47 to 62 Ma and exhibit well expressed very long eccentricity cycle minima [*Lourens et al.*, 2005; *Westerhold et al.*, 2007, 2008; *Westerhold and Röhl*, 2009]. Most important, within this rigid stratigraphic framework, the two data sets can only be moved in 405-kyr steps.

[11] In order to secure the connection between Site 1258 and 1262 we obtained additional XRF core scanning data for Site 1262 and generated stable bulk isotopes at certain intervals of Site 1258 to identify well known carbon isotope excursions H1 ('Elmo'), I1, and K ('X') [*Cramer et al.*, 2003; *Lourens et al.*, 2005; *Agnini et al.*, 2009; *Zachos et al.*, 2010].

3.1. Additional Bulk δ^{13}C and XRF Core Scanning Data

[12] Stable isotope measurements on 218 powdered (freeze-dried) bulk sediment samples from ODP Site 1258 were performed on a Finnigan MAT 251 mass spectrometer equipped with an automated carbonate preparation line at MARUM - University Bremen. The carbonate was reacted with orthophosphoric acid at 75°C. Analytical precision based on replicate analyses of in-house standard (Solnhofer Limestone) averages 0.05‰ (1σ) for δ^{13}C and 0.07‰ (1 σ) for δ^{18}O. All data are reported against VPDB after calibration of the in-house standard with NBS-19 and available in Table S1 in the auxiliary material.[1]

[13] XRF data were collected every 2 cm down-core over a 1 cm^2 area using 30 s count time directly at the split core surface of the archive half with XRF Core Scanner I and II (AVAATECH Serial No. 1 and 2) at the MARUM - University of Bremen [*Röhl and Abrams*, 2000; *Röhl et al.*, 2007; *Tjallingii et al.*, 2007; *Westerhold et al.*, 2007]. We scanned along the shipboard composite depth section (mcd) from 104.59 to 111.08 mcd [*Shipboard Scientific Party*, 2004]. All XRF core scanning Fe intensity data are reported in Table S2.

[14] Detailed comparison of the Fe intensity and bulk δ^{13}C data of ODP Sites 1258 and 1262 (Figure 3) reveal a doubling of sediment due to a fault at

[1]Auxiliary materials are available in the HTML. doi:10.1029/2012GC004096.

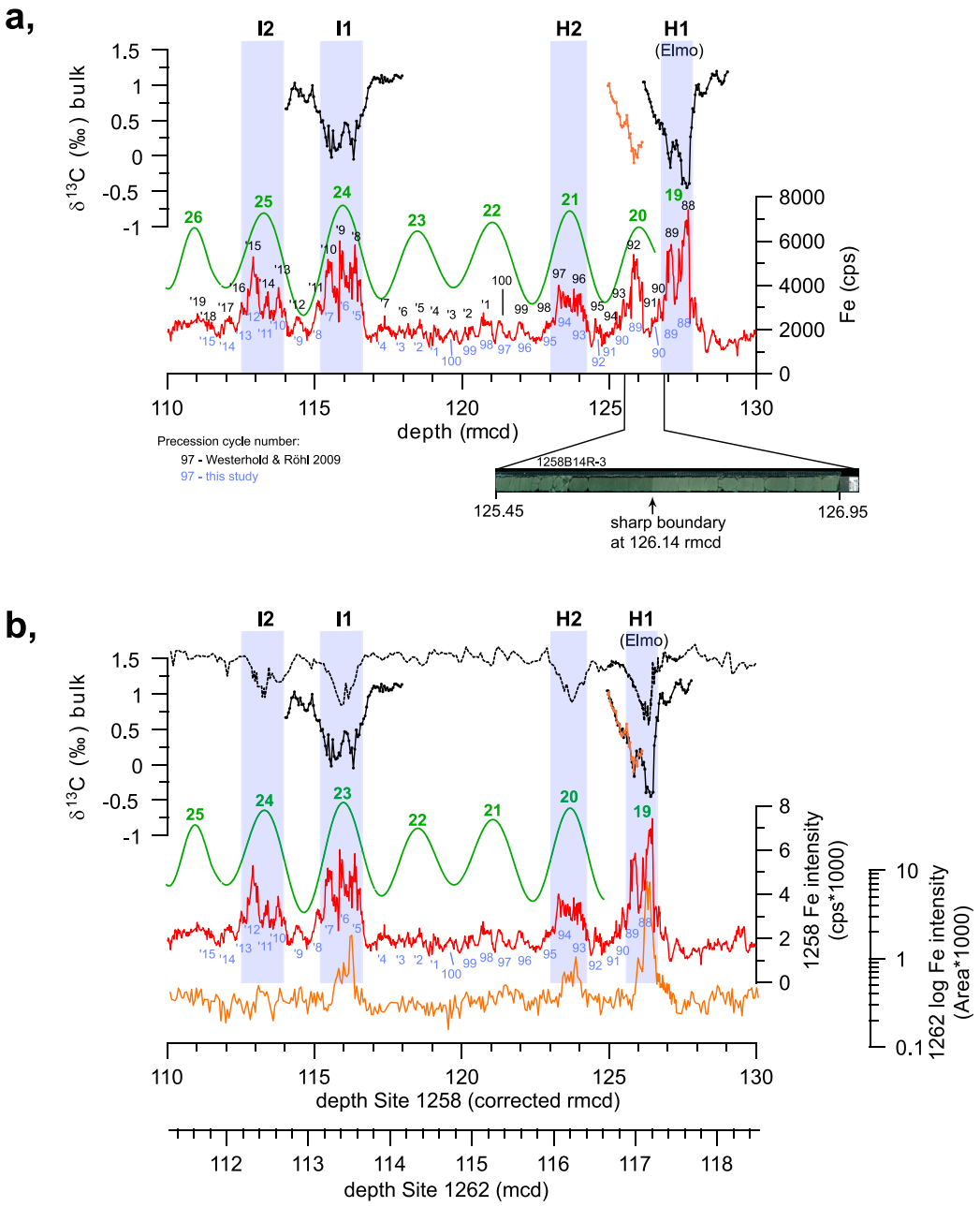

Figure 3. Corrected cyclostratigraphy for ODP Site 1258 based on comparison to Site 1262 XRF Fe intensity and bulk δ^{13}C data. Site 1258 XRF core scanning Fe intensity data [*Westerhold and Röhl*, 2009] (red) and bulk δ^{13}C data in per mill on specific intervals plotted in the depth and corrected depth domain. In green the filter output of the proposed 100-kyr eccentricity cycle (0.39 ± 0.12 cycles/meter) [*Westerhold and Röhl*, 2009] and the short eccentricity cycle number counted from the onset of the PETM are given [*Westerhold et al.*, 2007]. The smaller numbers are previous [*Westerhold and Röhl*, 2009] and corrected (blue) precession cycle counting estimates. The blue bars mark well known early Eocene carbon isotope excursions [*Cramer et al.*, 2003; *Lourens et al.*, 2005]. (a) All data on revised composite depth (rmcd). Observation of the Fe intensity and bulk δ^{13}C data show very similar patterns before (brown) and after (black) 126.14 rmcd suggesting a doubling of sediment due to a fault. This is confirmed by the presence of a sharp boundary at 126.14 rmcd as seen in the core image of 1258B14R-3. (b) Site 1258 data plotted on corrected rmcd by removing 1.22 m of doubled sediments. For comparison we plot the respective interval of Site 1262 XRF Fe intensity (orange, this study) and bulk δ^{13}C data (dashed black [*Zachos et al.*, 2010]). The almost identical pattern of the Site 1258 bulk δ^{13}C data from below (black) and above (brown) the sharp boundary indeed suggests a doubling of sediment. As a consequence the 100-kyr filter provides one cycle less between H1 and I1 but does not affect the number of 405-kyr cycles previously identified in 1258.

126.14 rmcd in Core 1258B-14R. About 1.22 m of the sedimentary succession has been doubled by the fault. A similar feature which might indicate another doubling of sediment in the section was not observed. Consequently the cyclostratigraphy for ODP Site 1258 [*Westerhold and Röhl*, 2009] was revised. The 100-kyr filter (see Figure 3) indicates that one short eccentricity cycle less is present between H1 and I1 as proposed before. The revision results in a one step shift in the short eccentricity cycle numbers from $E_{100}21$ to $E_{100}86$ (e.g., $E_{100}21$ shifts to $E_{100}20$). It is important to note that the above correction by one short eccentricity cycle does not affect the number of 405-kyr cycles previously identified at Site 1258 [*Westerhold and Röhl*, 2009].

4. Astronomical Calibration of the Paleocene and Early Eocene

[15] The well expressed very long eccentricity cycle in the XRF core scanning Fe data from ODP Site 1258 and 1262 provide the unique opportunity (1) to test the La2010 and La2011 solutions in the stable part from 47 to 54 Ma and (2) to anchor the floating stratigraphic framework for the Paleocene and early Eocene to obtain accurate absolute ages. The basic age model for this comparison is the consistent recognition of the number of stable 405-kyr cycles in the geological data [*Lourens et al.*, 2005; *Westerhold and Röhl*, 2006; *Westerhold et al.*, 2007, 2008; *Hilgen et al.*, 2010] from 47 to 60 Ma. This cyclostratigraphic framework can be shifted by 405-kyr increments in time.

4.1. Testing the Stability of the La2010 and La2011 Solutions

[16] Before we can start the test we need to know the phase relationship between $\delta^{13}C$, Fe intensity data and eccentricity. Bulk $\delta^{13}C$ data from ODP Site 1258 and 1262 show that minima in $\delta^{13}C$ correspond with peaks in Fe (i.e., carbonate dissolution), both of which appear to be in phase with maxima in eccentricity [*Lourens et al.*, 2005; *Zachos et al.*, 2010]. A very similar relation has been documented for the Oligocene and Miocene [*Zachos et al.*, 2001; *Pälike et al.*, 2004, 2006a, 2006b; *Holbourn et al.*, 2007] as well as the Paleocene and late Cretaceous [*Herbert*, 1997; *Zachos et al.*, 2010; *Westerhold et al.*, 2011]. At ODP Site 1258 and 1262 the sedimentary cyclicity is dominated by precession modulated by the short and long eccentricity cycles. The astronomical phase relationship is well documented [*Lourens et al.*, 2005] suggesting that the short and long eccentricity cycle are expressed in amplitude variations in the data. This way, large amplitude variations in Fe intensity data reflect large amplitude variations in orbital eccentricity and vice versa. Hence, minima in the very long eccentricity cycle will be expressed by very low amplitude modulations in the Fe intensity data and can be used as a distinctive fingerprint [*Lourens et al.*, 2005; *Westerhold et al.*, 2007].

[17] An astronomically tuned framework beyond 50 Ma can only be based on the identification of the stable long eccentricity cycle (405-kyr) [*Laskar et al.*, 2004] and not on the direct tuning to the short eccentricity cycle. Therefore, we establish a modified minimal tuning age model for Site 1262 similar to Site 1258. This minimal tuning assigns a tie point every 405-kyr based on the recognition and position of the long eccentricity cycle as given in the relevant publications [*Westerhold et al.*, 2007, 2008; *Westerhold and Röhl*, 2009]. We follow this approach to label the long eccentricity cycles in each epoch from the base to the top. The minimal tuning tie points are given in Table S3. We also extracted the amplitude modulation (AM) of the short eccentricity signal (95-kyr) of the orbital solutions and Fe intensity data of Sites 1258 and 1262 using the freeware ENVELOPE [*Schulz et al.*, 1999].

[18] We start the comparison with plotting the data and the extracted 95-kyr amplitude modulation of the data on the stable cyclostratigraphic framework using the modified option 1 age model [*Westerhold et al.*, 2007], with the onset of the PETM at 55.53 Ma. Subsequently we shift the records by 405-kyr steps to age model option 2 and option 3 moving the onset of the PETM to 55.93 Ma and 56.33 Ma, respectively (Figure 4). The best match of the 95-kyr AM between the orbital solutions and the Fe intensity data is obtained (Figure 5) choosing tuning option 1 for Sites 1258 and 1262 [*Westerhold et al.*, 2007, 2008; *Westerhold and Röhl*, 2009]. Especially the eccentricity cycle minima in the La2010a, La2010d and La2011 solutions are consistent with the geological data applying tuning option 1 (Figure 5). Linear correlation coefficients between orbital solutions and geological data also reveal that age model option 2 and option 3 show a significant mismatch to the solutions between 47 and 54 Ma (Figures 4 and 5 and Table 1). The comparison to Site 1262 does not show a clear picture. This empathizes that none of the orbital models are correct beyond 52 to 54 Ma. To evaluate the match between Site 1262 data and orbital solutions

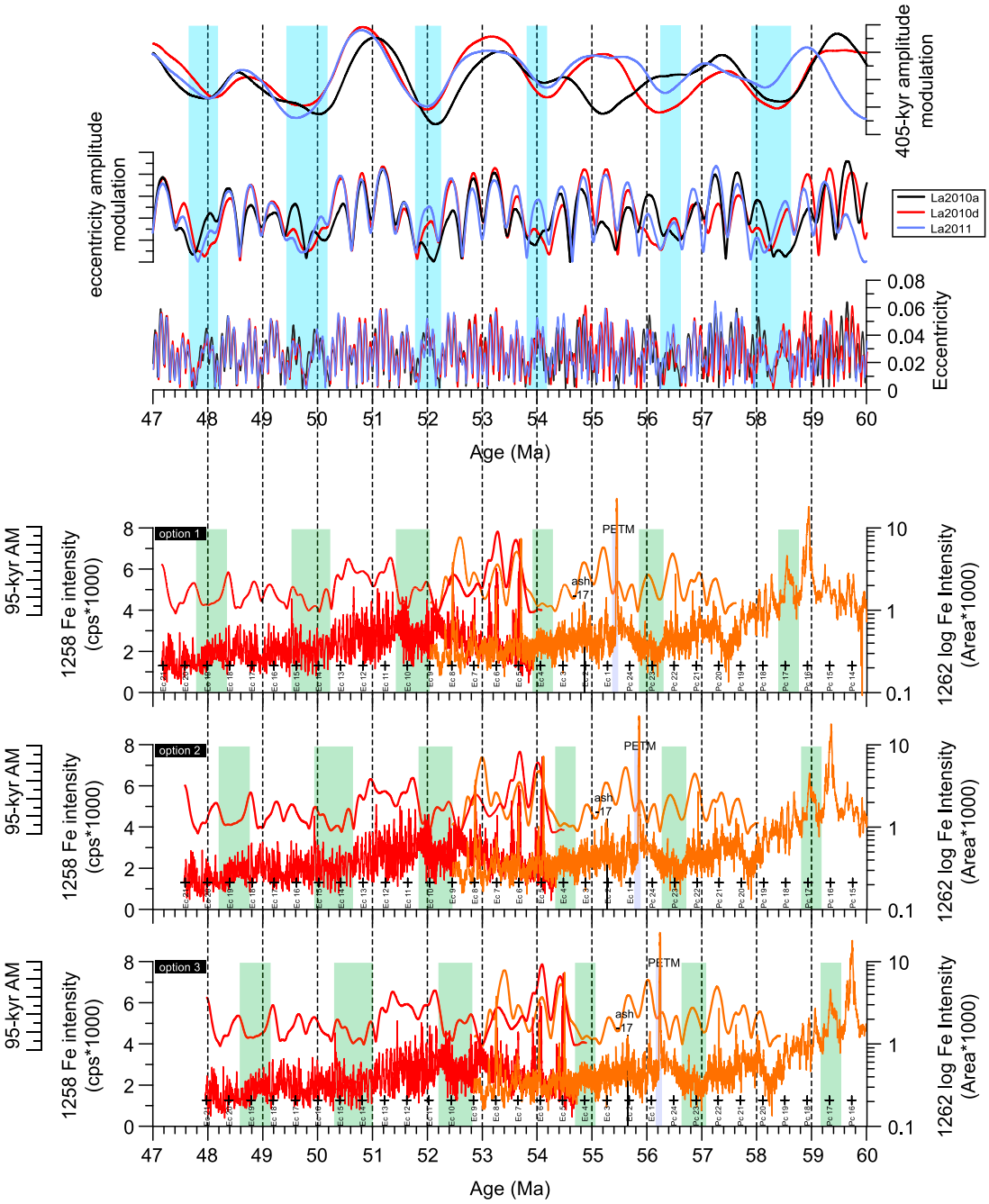

Figure 4. Comparison of the very-long eccentricity cycle minima between the geological data (XRF core scanning Fe intensity data from ODP Sites 1258 in red and 1262 in orange) and the La2010a, La2010d, La2011 orbital solutions. Top shows the different eccentricity solutions as well as the eccentricity and 405-kyr modulations. The lower three panels plot Fe intensity data and the extracted amplitude modulation (AM) of the short eccentricity (95-kyr AM) on three minimal tuning age scale options (Table S3), each offset by 405-kyr. Also given is the position and label of the long eccentricity (405-kyr) cycles identified in the geological data. Because the data are fixed in a stable 405-kyr stratigraphic framework the records can only be moved in 405-kyr steps in time. ~2.4 myr minima are highlighted by light blue bars in the orbital solutions and light green bars in the 1258 and 1258 Fe intensity data. The minima are expressed in the data as intervals of low variability in Fe intensity data and low 95-kyr AM. In addition, the resulting position of the PETM and ash −17 are given. This figure shows that moving the Fe intensity data sets to the option 2 or 3 age model will be inconsistent to the La2010d and La2011 solution with respect to the position of the very long eccentricity minima. Only option 1 provides an acceptable match to the stable part of the La2010d and La2011 solutions from 47 to 54 Ma.

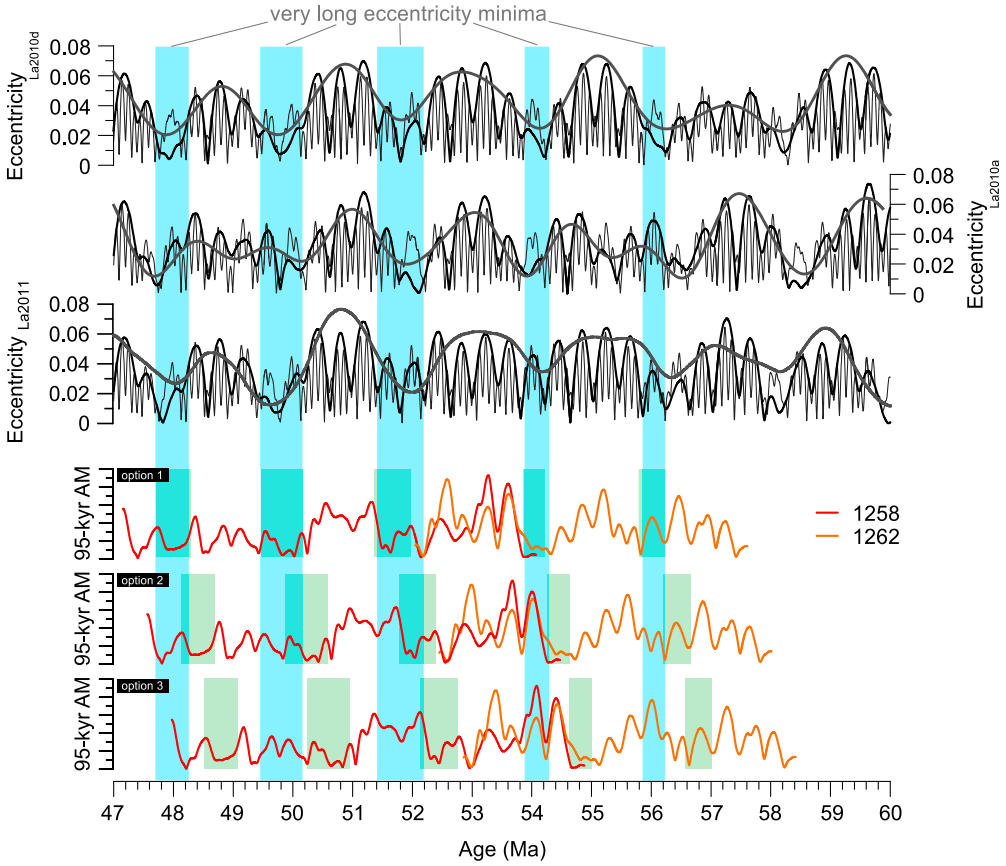

Figure 5. Comparison of the amplitude modulation (AM) of the short eccentricity cycle (95-kyr band) between the La2010d, La2010a, La2011 orbital solutions and Fe intensity data from ODP Sites 1258 (red) and 1262 (orange). For the orbital solutions we also plotted the 405-kyr AM. The 95-kyr AM of Site 1258 and 1262 Fe intensity data are plotted on the three minimal tuning age scale options (Table 3). ~2.4 myr minima are highlighted by light blue bars in the orbital solutions and light green bars in the 95-kyr AM of the 1258 and 1258 Fe intensity data. Best match (Table 1) between orbital solution and geological data are obtained using tuning option 1 in the stable interval from 47 to 54 Ma.

for the likely stable part of the orbital solutions we calculated the correlation coefficient from 52 to 55 Ma (Table 1). The evaluation reveals the best match is obtained between Site 1262 and all three orbital solutions using tuning option 1.

[19] Very long eccentricity minima in the Fe data are present at around 48.0 Ma, 49.8 Ma, 51.9 Ma and 54.1 Ma, which are consistent with the La2010d and La2011 solutions. These findings suggest that geologic data confirm the stability of the La2011 solution as far back as 54 Ma. The very long eccentricity minima at 51.9 Ma and 54.1 Ma are close to the onset of instability in the La2011 solution. But geological data indicate that the minima are indeed at the correct position. Any match beyond 54 Ma cannot be evaluated because of the high uncertainty of the eccentricity solutions older than 54 Ma. Moreover, the detailed comparison shows that geological data are better represented by La2010d and La2011 than by La2010a (Figure 5). This is in good agreement with the otherwise understanding that the long-term behavior of La2010d is more reliable than the one of La2010a,b,c suggesting that only La2010d and La2011 should be used beyond 47 Ma.

Table 1. Linear Correlation Coefficient of the 95-kyr Amplitude Modulation Between Orbital Solutions and Fe Intensity Data of ODP Sites 1258 and 1262

	1258			1262		
	Option1	Option2	Option3	Option1	Option2	Option3
Comparison of Entire Dataset Dominated by Precession Cycles						
La2010a	0.55	0.19	−0.16	0.16	0.07	0.39
La2010d	0.60	0.24	−0.19	0.46	0.31	0.08
La2011	0.55	0.26	0.01	0.32	0.39	0.38
Comparison of 1262 Dataset From 52 to 55 Ma						
La2010a				0.34	0.07	0.13
La2010d				0.56	0.19	−0.04
La2011				0.41	0.20	0.27

[20] Because of the growing uncertainty in the expression and shape of short eccentricity cycles in the very long eccentricity minima after 50 Ma we refuse to compare or even try to tune geological data to the short eccentricity cycles of the La2010 and La2011 solution. Due to this uncertainty a tuning of the early Eocene record of Site 1262 to the short eccentricity pattern is not possible. Unfortunately, for the same reason a comparison cannot resolve if there are 19 or 20 short eccentricity cycles between the onset of the PETM and the Elmo event [*Lourens et al.*, 2005; *Westerhold et al.*, 2007]. To do so an orbital solution is required that has a very small uncertainty in the short eccentricity cycle amplitude pattern in the very long eccentricity node at 54 Ma.

4.2. Paleocene and Early Eocene Astronomical Time Scale to La2010 and La2011

[21] Anchoring the geological data by minimal tuning age model option 1 results in the finding that an age estimate of ~56.0 Ma for the PETM [*Kuiper et al.*, 2008; *Hilgen et al.*, 2010] has to be rejected. The first-order age calibration to the very long eccentricity cycle minima in the La2011 solution suggests that tuning option 1 is correct for Sites 1262 [*Westerhold et al.*, 2007, 2008] and 1258 [*Westerhold and Röhl*, 2009]. Calibration to the very long eccentricity nodes proposes an absolute age of 55.53 ± 0.05 Ma for the onset of the PETM (Figure 6 and Table 2). Additionally, we obtain an astronomically tuned age of 54.85 Ma ± 0.05 Ma for ash −17, a well-dated prominent ash layer in the Fur Formation of Denmark [*Storey et al.*, 2007]. This ash layer has been tied to ODP Site 1262 by a detailed cyclostratigraphy procedure [*Westerhold et al.*, 2009]. Independent $^{40}Ar/^{39}Ar$ dating of ash −17 [*Storey et al.*, 2007] resulted in an age of 55.473 ± 0.120 Ma, calculated to an FC standard age of 28.201 Ma [*Kuiper et al.*, 2008] (Table 2). The comparison of radioisotopic to astronomical ages reveals a substantial discrepancy of 473 to 773 kyr.

5. Consequences for the Fish Canyon Radioisotopic Dating Standard

[22] Radioisotopic $^{40}Ar/^{39}Ar$ dating depends on the accuracy of the FC standard monitor age, the decay constant, and the precision of the measurement [*Renne et al.*, 1998]. Using FC ages of 28.02 Ma [*Renne et al.*, 1998], 28.201 Ma [*Kuiper et al.*, 2008] or 28.305 Ma [*Renne et al.*, 2010] results in significantly older ages for ash −17 and the PETM compared to the astronomically calibrated age (Figure 7 and Table 2). Although detailed biostratigraphy and cyclostratigraphy patterns indicate that the cyclostratigraphic position of ash −17 is correct [*Westerhold et al.*, 2009], a lower number of cycles between ash −17 and the PETM has been proposed [*Hilgen et al.*, 2010]. If the position of ash −17 with respect to the onset of the PETM is displaced by an order of 120–250 kyr [*Hilgen et al.*, 2010] (55.02–55.15 Ma), then the age of the PETM is still within the estimate using 28.02 Ma [*Renne et al.*, 1998] for the FC, but clearly younger than the estimates using 28.201 [*Kuiper et al.*, 2008] or 28.305 [*Renne et al.*, 2010] Ma (Table 2). Assuming that our astronomical age of ash −17 is correct, we recalculate an age of 27.89 Ma for the FC. This is within the error range of 28.02 ± 0.28 Ma [*Renne et al.*, 1998] and surprisingly close to the recent independent estimate of 27.93 Ma based on detailed and revised astronomical dating of the Pleistocene Matuyama-Brunhes boundary [*Channell et al.*, 2010].

[23] The astronomically tuned absolute age of the onset of the PETM is independent of the relative distance to ash −17 and its radioisotopic age. Recently, a high-precision U/Pb single-crystal zircon age for an ash layer within the PETM from Spitsbergen provided an estimate of 55.829 ± 0.10 Ma [*Charles et al.*, 2011]. This is ~300 kyr older than the astronomically calibrated age and supports the findings that U/Pb dates are systematically older than $^{40}Ar/^{39}Ar$ dates [*Min et al.*, 2000; *Schoene and Bowring*, 2006; *Schoene et al.*, 2006]. It should be noted that the U/Pb age of 55.785 ± 0.086 Ma for the lower bentonite in the Spitsbergen PETM is the weighted mean of the five youngest analyses. If the youngest single zircon age of 55.71 ± 0.14 Ma [*Charles et al.*, 2011] (55.57–55.85) approximates the eruption age, then the onset of the PETM is 55.61–55.89 Ma. This is close to but still 30–360 kyr older than the astronomical age, and might be related to residence time issues of zircon crystals [*Min et al.*, 2000; *Simon et al.*, 2008].

[24] Recalculations of various radioisotopic $^{40}Ar/^{39}Ar$ ages for the K/Pg boundary, applying the revised estimate of 27.89 Ma for the FC, provide ages between 65.08 and 65.26 Ma (Table 2), which are consistent with the 65.28 Ma estimate from tuning option 1 of the Paleocene time scale [*Westerhold et al.*, 2008]. The duration of the Paleocene Epoch based on the astronomically calibrated age for the PETM and the recalculated

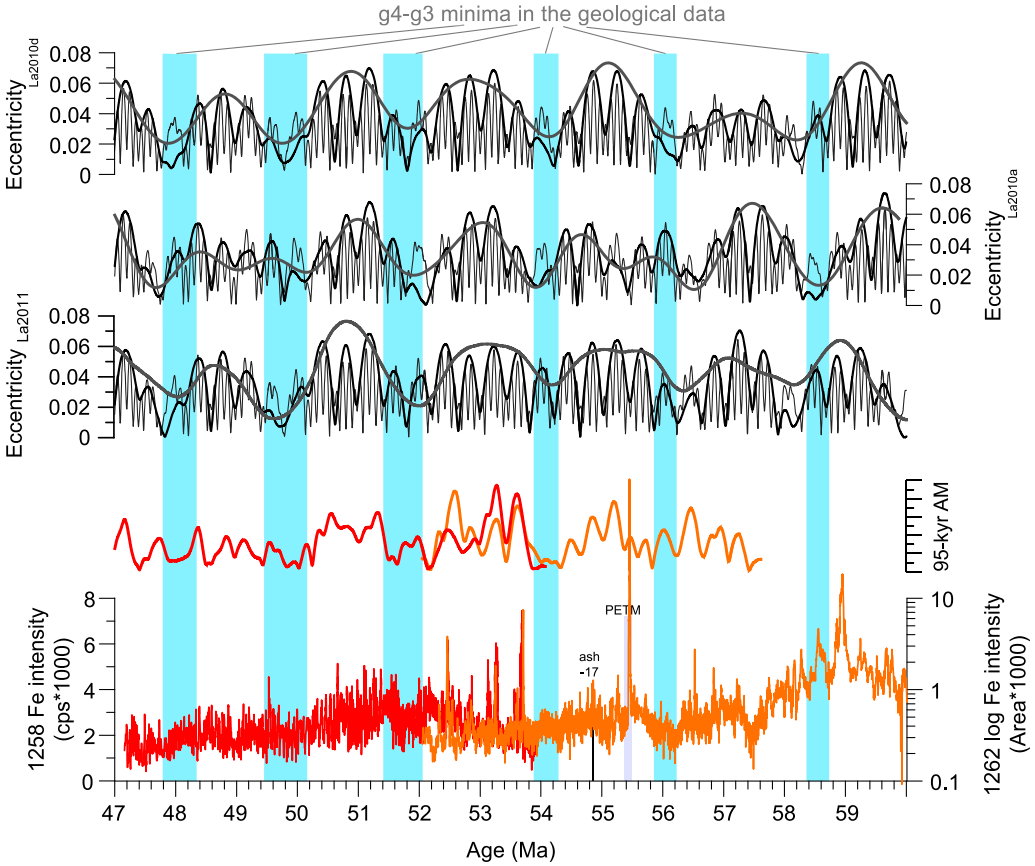

Figure 6. Eccentricity solution La2010a, La2010d (both [*Laskar et al.*, 2011a]) and La2011 [*Laskar et al.*, 2011b] of the Earth (fine black line) compared to paleoclimate stratigraphic data to assess the positions of the very long eccentricity cycle minima from 47 to 60 Ma. To accentuate successive minima in the eccentricity solution the amplitude modulation was extracted from the orbital solution (thick black line). The 95-kyr AM of Site 1258 (red) and 1262 Fe (orange) intensity data are plotted on tuning option 1. The light blue bars mark the very long eccentricity minima in the orbital solutions and the geological data. Those records are XRF core scanning iron (Fe) intensity data from ODP Sites 1262 (orange) [*Westerhold et al.*, 2007, 2008] and 1258 (red) [*Westerhold and Röhl*, 2009] which are dominated by eccentricity modulated precession cycles. Both data sets are plotted on a floating stable 405-kyr cyclostratigraphic framework that can only be shifted by 405-kyr steps. The framework shows the best fit of the very long eccentricity minima between La2010a, La2010d, La2011 and the geological data from 47 to 54 Ma. However, shifting the framework 405-kyr older or younger will result in substantial mismatches with current orbital solutions La2010a, La2010d and La2011 (see Figure 4). Also given is the position of the Paleocene/Eocene Thermal Maximum (PETM) [*Westerhold et al.*, 2007] and ash −17 [*Westerhold et al.*, 2009].

radioisotopic ages for the K/Pg boundary is between 9.55 and 9.75 myr, suggesting that the entire Paleocene contains 24 [*Westerhold et al.*, 2008] 405-kyr eccentricity cycles, not 25 [*Hilgen et al.*, 2010]. Retuning of the Paleocene time scale to the La2011 405-kyr cycle results in an age of 65.25 ± 0.06 Ma for the K/Pg boundary.

6. The Astronomical Calibration Controversy

[25] Our findings in the early Eocene and those of *Channell et al.* [2010] for Pleistocene sediments point to a problem in the stratigraphic interpretation at the Sorbas section (Spain) [*Krijgsman et al.*, 1999] and the subsequent correlation of these sediments to those of the Messâdit section (Melilla Basin, NE Morocco) [*Sierro et al.*, 2001; *van Assen et al.*, 2006] used for the recalibration of the age of the Fish Canyon sanidine [*Kuiper et al.*, 2008]. Critical to the astrochronologic calibration of the Messâdit section is the recognition of planktonic foraminiferal events [*van Assen et al.*, 2006]. Although the correlation of these events may be in error as the temporal ranges of the fauna are not that well defined (see discussion in *Channell et al.* [2010]), the number of identified cycles between events is similar to astronomically calibrated Mediterranean sections

Table 2. Recalculated Radioisotopic Ages

	Age Ma	FC 27.89[a]	FC 27.93[b]	FC 28.02[c]	FC 28.201[d]	FC 28.305[e]
	Astronomically Calibrated Absolute Age					
Onset PETM[a]	55.530 ± 0.05					
Ash -17[l]	54.850 ± 0.05					
		Ash-17				
Ar/Ar age[f] (±0.120 kyr)		54.866	54.944	55.120	55.473	55.676
Relative to onset PETM[g]	54.858 ± 0.05					
Relative to onset PETM[g,h]	54.900 ± 0.05					
		K/Pg Boundary				
BKSA1995	65.000					
GTS2004	65.500 ± 0.30					
Absolute age option 1[i]	65.280 ± 0.01					
Absolute age La2011[a]	65.250 ± 0.06					
Zumaia tuned[d]	65.957 ± 0.04					
Zumaia tuned[j]	65.777					
Beloc tektite, Haiti[k]		65.25	65.34		65.98 ± 0.20	
C1 glassy melt rock of Chicxulub crater[l]		65.08	65.17		65.81 ± 0.14	
IrZ-coal bentonite – sanidine[m]		65.26	65.35		65.99 ± 0.12	
Z-coal combined[m]		65.11	65.20		65.84 ± 0.12	

[a]This study.
[b]*Channell et al.* [2010].
[c]*Renne et al.* [1998].
[d]*Kuiper et al.* [2008].
[e]*Renne et al.* [2010].
[f]*Storey et al.* [2007].
[g]*Westerhold et al.* [2009].
[h]*Murphy et al.* [2010].
[i]*Westerhold et al.* [2008].
[j]*Dinarès-Turell et al.* [2003].
[k]*Izett et al.* [1991].
[l]*Swisher et al.* [1992].
[m]*Swisher et al.* [1993].

[*Krijgsman et al.*, 1999; *Hilgen et al.*, 2000a; *Krijgsman et al.*, 2001; *Sierro et al.*, 2001] that form the core of the Geomagnetic Polarity Time Scale (GPTS) for the late Miocene, especially magnetochrons C3An.1n to C3Bn [*Lourens et al.*, 2004].

[26] Recently, the $^{40}Ar/^{39}Ar$ FC age of 28.201 ± 0.046 Ma [*Kuiper et al.*, 2008] has been confirmed by the astronomically intercalibrated age of 28.172 ± 0.028 Ma (2σ, external errors) obtained from the direct astronomically tuned A1 ash in the Faneromeni section (Crete) [*Rivera et al.*, 2011]. The A1 tephra is located at the base of sapropel FC28 about in the middle of magnetic polarity chron C3Ar [*Krijgsman et al.*, 1994; *Hilgen et al.*, 1997; *Kuiper et al.*, 2004]. The astronomical tuning of the Faneromeni section is thought to be straight forward and consistent with other Mediterranean sections [*Hilgen et al.*, 1995]. The initial age for A1 of 6.941 ± 0.005 Ma [*Hilgen et al.*, 1997; *Kuiper et al.*, 2004] was slightly revised to 6.943 ± 0.005 Ma [*Rivera et al.*, 2011] applying the La2004 solution for precession and obliquity and the La2010 solution for eccentricity. Therefore, the study of *Rivera et al.* [2011] supports the biostratigraphic correlation applied to the Messâdit section [*van Assen et al.*, 2006; *Kuiper et al.*, 2008] and seems to independently confirm the astronomical tuning of the Sorbas section [*Krijgsman et al.*, 1999].

[27] In this context, our results are highly controversial to those obtained from the Mediterranean sections. Absolutely crucial, however, for the approach of *Kuiper et al.* [2008] and *Rivera et al.* [2011] is an absolutely perfect analysis of cyclicity expressed in the road-cut outcrops at the Sorbas and the Faneromeni section. Land sections are often more difficult to interpret than the multiple hole and transect approach of ODP sediment cores. It is essential to note that a small error in the tuning of 20 kyr around 6.5–7.0 Ma will increase by an order of magnitude to a mismatch of more than 200 kyr at 50 to 60 Ma. With respect to our new result for the absolute age of ash −17, the PETM and the K/Pg boundary this possibly indicates a likely tuning

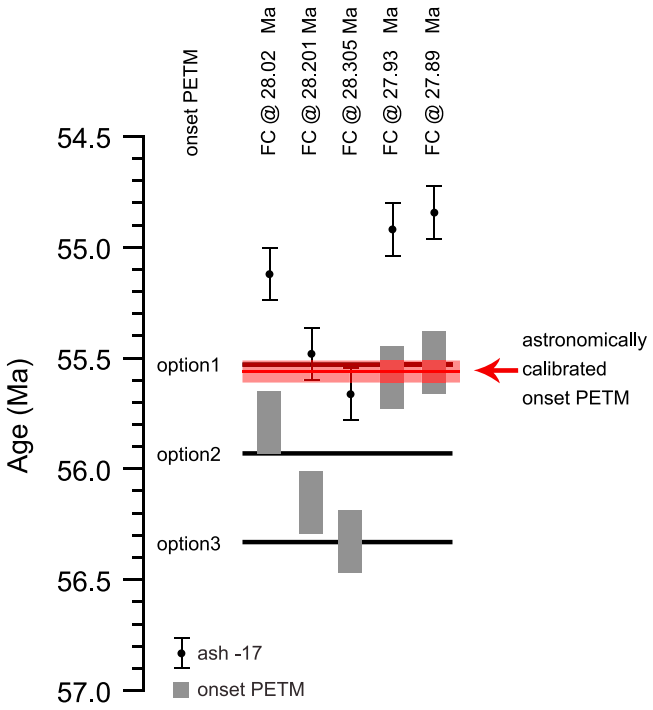

Figure 7. Comparison of astronomical and radioisotopic ages for the Paleocene/Eocene Thermal Maximum (PETM). Gray bars mark the absolute age range for the onset of the PETM based on the age and relative distance of ash −17 with respect to the age of the Fish Canyon (FC) radiometric dating standard of 28.02 [*Renne et al.*, 1998], 28.201 [*Kuiper et al.*, 2008], 28.305 [*Renne et al.*, 2010], 27.93 [*Channell et al.*, 2010], and 27.89 (this study) Ma. Horizontal black lines mark the three possible options of the age range for the onset of the PETM based on the astronomically calibrated Paleocene time scale [*Westerhold et al.*, 2008]. The red bar and arrow mark the new astronomically calibrated absolute age for the onset of the PETM established in this study by anchoring the geological data to the La2011 [*Laskar et al.*, 2011b] eccentricity solution.

error for the Faneromeni and Messâdit section of 40–60 kyr or 2–3 precession cycles. This error is much larger than any error introduced by possible local phase relation changes to precession and/or obliquity [*Laepple and Lohmann*, 2009]. Tuning the sections 60 kyr too old will lead to 0.8% older $^{40}Ar/^{39}Ar$ ages than expected if using the 28.02 Ma (or 27.9 Ma argued for here) age for the Fish Canyon sanidine.

6.1. Tuning of the Sorbas, Faneromeni and Messâdit Sections

[28] The tuning of the Sorbas and Faneromeni sections is thought to be robust because the observed sapropel pattern exactly matches precession/obliquity interference patterns in the interval from C3An.1n to C3Bn [*Krijgsman et al.*, 1999] and the overall cyclostratigraphic correlation to the long and short eccentricity cycles is well established [*Hilgen et al.*, 1995]. Nevertheless, looking into detail reveals some discrepancies that might indicate that the tuning of these sections is not absolutely correct down to the individual precession cycle as required for refining the FC.

[29] The tuning of the Sorbas section [*Krijgsman et al.*, 1999] was based on the age of magnetochron C3An.1n of the previously established 'tuning' of the early Messinian [*Hilgen et al.*, 1995]. But this age was not obtained by direct orbital tuning due to the absence of tunable sections in the Mediterranean from 6.7–5.3 Ma [*Hilgen*, 1991]. Instead it was established by linear interpolation of seafloor spreading rates between the top of C3n.4n and the top of C3An.2n [*Hilgen et al.*, 1995] (see Table 3). The age of the top of C3n.4n is well established and consistent with seafloor spreading rate changes [*Wilson*, 1993; *Cande and Kent*, 1995; *Lourens et al.*, 1996; *Lourens et al.*, 2004]. The age of 6.677 Ma for the top of C3An.2n in *Hilgen et al.* [1995] is based on tuning of the Faneromeni section and correlation between the Kastelli (Crete), Metochia (Gavdos), and Giblescemi (Sicily) sections. Tuned ages for magnetochrons older than C4n.1n (7.528 Ma) have been confirmed [*Hüsing*

Table 3. Differences in Geomagnetic Polarity Time Scale Calibrations

	Age in Ma			Δ (in kyr)		
Chron	ATNTS/GPTS2004	*Cande and Kent* [1995]	*Hilgen et al.* [1995]	ATNTS-CK95	ATNTS-H95	CK95-H95
C3n.1n (y)	4.187	4.180	4.188[c]	0.007	−0.001	−0.008
C3n.1n (o)	4.300	4.290	4.300[c]	0.010	0.000	−0.010
C3n.2n (y)	4.493	4.480	4.493[c]	0.013	0.000	−0.013
C3n.2n (o)	4.631	4.620	4.632[c]	0.011	−0.001	−0.012
C3n.3n (y)	4.799	4.800	4.799[c]	−0.001	0.000	0.001
C3n.3n (o)	4.896	4.890	4.896[c]	0.006	0.000	−0.006
C3n.4n (y)	4.997	4.980	4.998[c]	0.017	−0.001	−0.018
C3n.4n (o)	5.235	5.230	5.236[c]	0.005	−0.001	−0.006
C3An.1n (y)	**6.033**[a]	**5.894**	***5.952***[d]	**0.139**	**0.081**	**−0.058**
C3An.1n (o)	**6.252**[a]	**6.137**	***6.214***[d]	**0.115**	**0.038**	**−0.077**
C3An.2n (y)	**6.436**[a]	**6.269**	***6.356***[d]	**0.167**	**0.080**	**−0.087**
C3An.2n (o)	**6.733**[a]	**6.567**	**6.677**[e]	**0.166**	**0.056**	**−0.110**
C3Bn (y)	**7.140**[b]	**6.935**	**7.101**[e]	**0.205**	**0.039**	**−0.166**
C3Bn (o)	7.212[b]	7.091	7.210	0.121	0.002	−0.119
C3Br.1n (y)	7.251[b]	7.135	7.256	0.116	−0.005	−0.121
C3Br.1n (o)	7.285[b]	7.170	7.301	0.115	−0.016	−0.131
C3Br.2n (y)	7.454	7.341	7.455	0.113	−0.001	−0.114
C3Br.2n (o)	7.489	7.375	7.492	0.114	−0.003	−0.117
C4n.1n (y)	7.528	7.432	7.532	0.096	−0.004	−0.100
C4n.1n (o)	7.642	7.562	7.644	0.080	−0.002	−0.082
C4n.2n (y)	7.695	7.650	7.697	0.045	−0.002	−0.047
C4n.2n (o)	8.108	8.072	8.109	0.036	−0.001	−0.037
C4r.1n (y)	8.254	8.225	8.257	0.029	−0.003	−0.032
C4r.1n (o)	8.300	8.257	8.303	0.043	−0.003	−0.046
C4An (y)	8.769	8.699	8.750	0.070	0.019	−0.051

[a]*Krijgsman et al.* [1999] – Sorbas section.
[b]*Hilgen et al.* [2000b] – Oued Akrech section.
[c]*Lourens et al.* [1996].
[d]Based on linear interpolation of seafloor spreading rates between C3n.4n (o) and C3An.2n (o) [*Hilgen et al.*, 1995].
[e]*Hilgen et al.* [1995].

et al., 2007, 2009], but ages for C4An.1n to C3An.1n are uncertain because sedimentary succession cannot clearly be related to orbital cycles in the Faneromeni, Kastelli and Metochia sections [*Hilgen et al.*, 1995]. Therefore, the age of the top of C3An.1n used for the initial tuning of the Sorbas section could be questioned. In fact, the age of C3An.1n (o) in *Hilgen et al.* [1995] is 58 kyr older than CK95 [*Cande and Kent*, 1992; 1995] and leads to 139 kyr older age after tuning of the Sorbas section [*Krijgsman et al.*, 1999] (Table 3). The combination of the tuned magnetostratigraphy of the Sorbas and the Abad composite (Sorbas and Nijar basin) [*Sierro et al.*, 2001] used in the ATNTS/GPTS2004 [*Lourens et al.*, 2004] even show a difference of up to 205 kyr with respect to CK95 at C3Bn (y), a discrepancy of almost 3%. Differences in the absolute ages for magnetochron C3r to C4n.2n (Table 3) can lead to some significant changes in seafloor spreading rates (Figure 8). We have calculated apparent changes in seafloor spreading rates using the distances of the South Atlantic spreading center [*Cande and Kent*, 1992] as done for the GPTS 2004 [*Ogg and Smith*, 2004]. The comparison shows minor to major differences to CK95 during chrons C3r to C4n.2n. Moderate changes in spreading rate are consistent with the ATNTS in the Pliocene [*Wilson*, 1993], but unknown thereafter. By far the highest peak in South Atlantic seafloor spreading rates during the entire Cenozoic occurs at chron C3Bn using the ATNTS/GPTS2004 [*Lourens et al.*, 2004; *Ogg and Smith*, 2004], around 7 Ma. This might point to potential errors in the astronomically calibrated time scale for C3An.1n to C4n.1n derived from the Sorbas basin sections. It is difficult to identify directly where the error in tuning might be because the correlation between the Sorbas, the Melillia basin and Cretian sections is complex. *Hodell et al.* [2001] established a correlation between the Mediterranean, ODP Site 982 (North Atlantic) and the Salé Briqueterie section (NW Marocco [*Hodell et al.*, 1994]), but rely for an initial age model on the astronomical ages for foraminiferal events derived from *Hilgen et al.* [1995]. Thus, an independent astronomically tuned interval spanning C3r to C4n.1n from outside the Mediterranean with

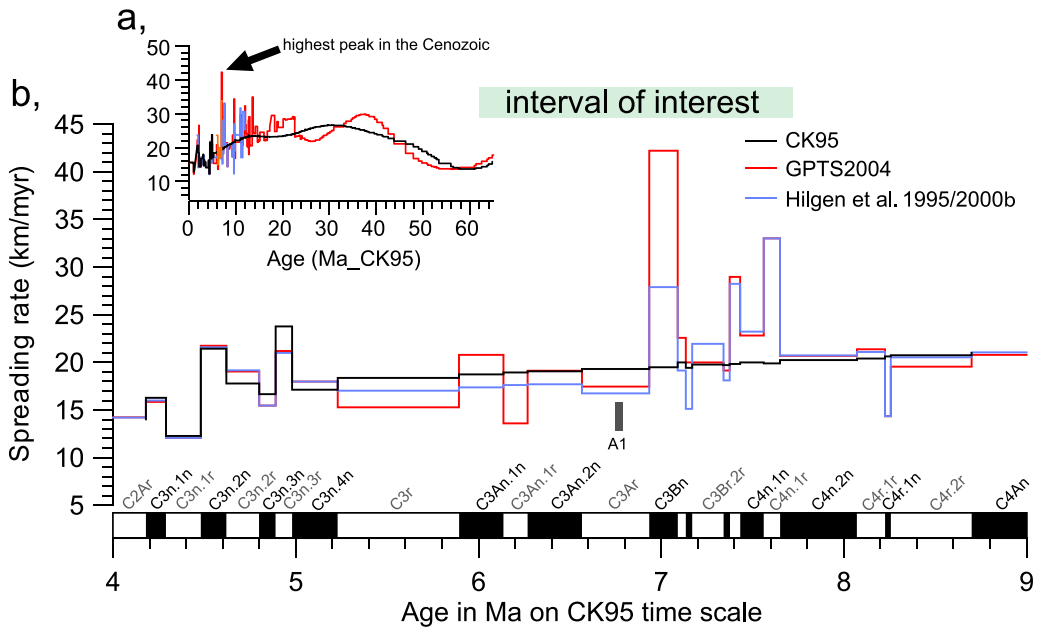

Figure 8. Comparison of calculated spreading rates for the synthetic South Atlantic profile of *Cande and Kent* [1992] based on the age model of *Cande and Kent* [1995] (black line), *Hilgen et al.* [1995, 2000b] (blue line), and Geomagnetic Polarity Time Scale 2004 (GPTS2004 [*Lourens et al.*, 2004], red line). All data are plotted on the CK95 age scale for simplified comparison. (a) Spreading rate for the entire Cenozoic era to illustrate the exceptional high peak at 7 Ma. (b) Spreading rates from 4 to 9 Ma with magnetostratigraphy. Also given, the relative position of the A1 ash layer from the Faneromeni section in chron C3Ar [*Hilgen et al.*, 1997]. The interval of interest marks the period where a perfect astronomical tuning is required to determine the accurate age of ash layers used for intercalibration between the astronomical and radio-isotopic dating method.

high quality magnetostratigraphy would be needed for final clarification.

7. Conclusions

[30] Geological data from deep-sea sediments confirm the exact positions of very long eccentricity minima in the new La2011 orbital solution from 47 to 54 Ma. For the first time, this allows direct correlation between geological data and a stable astronomical solution in the early Eocene independent from radioisotopic dating. First-order calibration of the geological data to the very long eccentricity minima in La2011 suggests that the astronomically calibrated absolute ages for ash −17, the PETM and the K/Pg boundary are in conflict with radioisotopically dated $^{40}Ar/^{39}Ar$ ages based on recently recalibrated Fish Canyon (FC) standard ages [*Kuiper et al.*, 2008; *Renne et al.*, 2010; *Rivera et al.*, 2011]. In contrast to a recent confirmation [*Rivera et al.*, 2011], but in line with the study of *Channell et al.* [2010], our results point to a 0.8% younger age for the FC of ~27.9 Ma than the *Kuiper et al.* [2008] estimate.

[31] Although the analytical precision of radioisotopic dating has improved tremendously, the discrepancy between the astronomical ages presented here and radioisotopic ages is profound. Our results point to intrinsic problems with the decay constants and/or standard ages used in $^{40}Ar/^{39}Ar$ dating, and possible biasing of the U-Pb clock in zircon crystals due to the memory of pre-eruption crystallization of magma that forms large volcanic ashfall deposits, or both. If so, the synchronization of $^{40}Ar/^{39}Ar$ and U/Pb radioisotopic clocks as proposed by *Kuiper et al.* [2008] is problematic.

[32] Our results indicate that the tuning of the late Miocene Mediterranean sections (Sorbas, Faneromeni, Messâdit, etc.), which contain the ash layers used for the intercalibration of the FC [*Kuiper et al.*, 2008; *Rivera et al.*, 2011], could be in error by 40–60 kyr. Independent astronomically tuned sections from outside the Mediterranean with high-quality magnetostratigraphy are required to solve the time scale controversy.

Acknowledgments

[33] We thank Monika Segl and her team for stable isotope analyses. We are indebted to H. Pfletschinger and V. Lukies (MARUM) for assisting in XRF core scanning. This research

used samples and data provided by the Integrated Ocean Drilling Program (IODP). IODP is sponsored by the U.S. National Science Foundation (NSF) and participating countries under the management of Joint Oceanographic Institutions (JOI), Inc. Financial support for this research was provided by the Deutsche Forschungsgemeinschaft (DFG), ANR-ASTCM, PNP-CNRS, and CS from Paris Observatory. We thank three anonymous reviewers who provided thoughtful and thorough reviews improving the paper. The data reported in this paper are tabulated in the auxiliary material and archived at the Pangaea database (doi.pangaea.de/10.1594/PANGAEA.783354).

References

Agnini, C., P. Macri, J. Backman, H. Brinkhuis, E. Fornaciari, L. Giusberti, V. Luciani, D. Rio, A. Sluijs, and F. Speranza (2009), An early Eocene carbon cycle perturbation at 52.5 Ma in the Southern Alps: Chronology and biotic response, *Paleoceanography*, *24*, PA2209, doi:10.1029/2008PA001649.

Cande, S. C., and D. V. Kent (1992), A new geomagnetic polarity time scale for the late Cretaceous and Cenozoic, *J. Geophys. Res.*, *97*(B10), 13,917–13,951.

Cande, S. C., and D. V. Kent (1995), Revised calibration of the geomagnetic polarity timescale for the Late Cretaceous and Cenozoic, *J. Geophys. Res.*, *100*(B4), 6093–6095, doi:10.1029/94JB03098.

Channell, J. E. T., D. A. Hodell, B. S. Singer, and C. Xuan (2010), Reconciling astrochronological and $^{40}Ar/^{39}Ar$ ages for the Matuyama-Brunhes boundary and late Matuyama Chron, *Geochem. Geophys. Geosyst.*, *11*, Q0AA12, doi:10.1029/2010GC003203.

Charles, A. J., D. J. Condon, I. C. Harding, H. Pälike, J. E. A. Marshall, Y. Cui, L. Kump, and I. W. Croudace (2011), Constraints on the numerical age of the Paleocene-Eocene boundary, *Geochem. Geophys. Geosyst.*, *12*, Q0AA17, doi:10.1029/2010GC003426.

Cramer, B. S., J. D. Wright, D. V. Kent, and M.-P. Aubry (2003), Orbital climate forcing of $\delta^{13}C$ excursions in the late Paleocene–early Eocene (chrons C24n–C25n), *Paleoceanography*, *18*(4), 1097, doi:10.1029/2003PA000909.

Dinarès-Turell, J., J. I. Baceta, V. Pujalte, X. Orue-Etxebarria, G. Bernaola, and S. Lorito (2003), Untangling the Paleocene climatic rhythm: An astronomically calibrated Early Paleocene magnetostratigraphy and biostratigraphy at Zumaia (Basque basin, northern Spain), *Earth Planet. Sci. Lett.*, *216*, 483–500, doi:10.1016/S0012-821X(03)00557-0.

Erbacher, J., et al. (2004), *Proceedings of the Ocean Drilling Program, Initial Reports*, vol. 207, Ocean Drill. Program, College Station, Tex.

Fienga, A., H. Manche, J. Laskar, and M. Gastineau (2008), INPOP06: A new numerical planetary ephemeris, *Astron. Astrophys.*, *477*(1), 315–327, doi:10.1051/0004-6361:20066607.

Fienga, A., J. Laskar, T. Morley, H. Manche, P. Kuchynka, C. Le Poncin-Lafitte, F. Budnik, M. Gastineau, and L. Somenzi (2009), INPOP08, a 4-D planetary ephemeris: From asteroid and time-scale computations to ESA Mars Express and Venus Express contributions, *Astron. Astrophys.*, *507*(3), 1675–1686, doi:10.1051/0004-6361/200911755.

Fienga, A., J. Laskar, P. Kuchynka, H. Manche, G. Desvignes, M. Gastineau, I. Cognard, and G. Theureau (2011), The INPOP10a planetary ephemeris and its applications in fundamental physics, *Celestial Mech. Dyn. Astron.*, *111*(3), 363–385, doi:10.1007/s10569-011-9377-8.

Gradstein, F., J. Ogg, and A. Smith (2004), *A Geological Timescale 2004*, Cambridge Univ. Press, Cambridge, U. K., doi:10.4095/215638.

Hay, W. W. et al. (1999), Alternative global Cretaceous paleogeography, in *The Evolution of Cretaceous Ocean/Climate Systems*, edited by E. Barrera and C. Johnson, *Spec. Pap. Geol. Soc. Am.*, *332*, 1–47, doi:10.1130/0-8137-2332-9.1.

Herbert, T. D. (1997), A long marine history of carbon cycle modulation by orbital-climatic changes, *Proc. Natl. Acad. Sci. U. S. A.*, *94*, 8362–8369, doi:10.1073/pnas.94.16.8362.

Hilgen, F. J. (1991), Astronomical calibration of Gauss to Matuyama sapropels in the Mediterranean and implication for the geomagnetic polarity time scale, *Earth Planet. Sci. Lett.*, *104*, 226–244, doi:10.1016/0012-821X(91)90206-W.

Hilgen, F. J. (2010), Astronomical dating in the 19th century, *Earth Sci. Rev.*, *98*(1–2), 65–80, doi:10.1016/j.earscirev.2009.10.004.

Hilgen, F. J., W. Krijgsman, C. G. Langereis, L. J. Lourens, A. Santarelli, and W. J. Zachariasse (1995), Extending the astronomical (polarity) time scale into the Miocene, *Earth Planet. Sci. Lett.*, *136*, 495–510, doi:10.1016/0012-821X(95)00207-S.

Hilgen, F. J., W. Krijgsman, and J. R. Wijbrans (1997), Direct comparison of astronomical and $^{40}Ar/^{39}Ar$ ages of ash beds: Potential implications for the age of mineral dating standards, *Geophys. Res. Lett.*, *24*(16), 2043–2046, doi:10.1029/97GL02029.

Hilgen, F. J., S. Iaccarino, W. Krijgsman, G. Villa, C. G. Langreis, and W. J. Zachariasse (2000a), The Global Boundary Stratotype Section and Point (GSSP) of the Messinian Stage (uppermost Miocene), *Episodes*, *23*(3), 172–178.

Hilgen, F. J., L. Bissoli, S. Iaccarino, W. Krijgsman, R. Meijer, A. Negri, and G. Villa (2000b), Integrated stratigraphy and astrochronology of the Messinian GSSP at Oued Akrech (Atlantic Morocco), *Earth Planet. Sci. Lett.*, *182*(3–4), 237–251, doi:10.1016/S0012-821X(00)00247-8.

Hilgen, F. J., K. F. Kuiper, and L. J. Lourens (2010), Evaluation of the astronomical time scale for the Paleocene and earliest Eocene, *Earth Planet. Sci. Lett.*, *300*(1–2), 139–151, doi:10.1016/j.epsl.2010.09.044.

Hodell, D. A., R. H. Benson, D. V. Kent, A. Boersma, and K. Rakic-El Bied (1994), Magnetostratigraphic, biostratigraphic, and stable isotope stratigraphy of an Upper Miocene drill core from the Salé Briqueterie (northwestern Marocco): A high-resolution chronology for the Messinian stage, *Paleoceanography*, *9*(6), 835–855, doi:10.1029/94PA01838.

Hodell, D. A., J. H. Curtis, F. J. Sierro, and M. A. Raymo (2001), Correlation of late Miocene to early Pliocene sequences between the Mediterranean and North Atlantic, *Paleoceanography*, *16*(2), 164–178, doi:10.1029/1999PA000487.

Holbourn, A., W. Kuhnt, M. Schulz, J.-A. Flores, and N. Andersen (2007), Orbitally paced climate evolution during the middle Miocene "Monterey" carbon-isotope excursion, *Earth Planet. Sci. Lett.*, *261*(3–4), 534–550, doi:10.1016/j.epsl.2007.07.026.

Hüsing, S. K., F. J. Hilgen, H. Abdul Aziz, and W. Krijgsman (2007), Completing the Neogene geological time scale between 8.5 and 12.5 Ma, *Earth Planet. Sci. Lett.*, *253*(3–4), 340–358, doi:10.1016/j.epsl.2006.10.036.

Hüsing, S. K., K. F. Kuiper, W. Link, F. J. Hilgen, and W. Krijgsman (2009), The upper Tortonian–lower Messinian at Monte dei Corvi (Northern Apennines, Italy): Completing a Mediterranean reference section for the Tortonian Stage,

Earth Planet. Sci. Lett., *282*(1–4), 140–157, doi:10.1016/j.epsl.2009.03.010.

Husson, D., B. Galbrun, J. Laskar, L. A. Hinnov, N. Thibault, S. Gardin, and R. E. Locklair (2011), Astronomical calibration of the Maastrichtian (Late Cretaceous), *Earth Planet. Sci. Lett.*, *305*(3–4), 328–340, doi:10.1016/j.epsl.2011.03.008.

Izett, G. A., G. B. Dalrymple, and L. W. Snee (1991), $^{40}Ar/^{39}Ar$ age of Cretaceous-Tertiary boundary tektites from Haiti, *Science*, *252*(5012), 1539–1542, doi:10.1126/science.252.5012.1539.

Krijgsman, W., F. J. Hilgen, C. G. Langereis, and W. J. Zachariasse (1994), The age of the Tortonian/Messinian boundary, *Earth Planet. Sci. Lett.*, *121*(3–4), 533–547, doi:10.1016/0012-821X(94)90089-2.

Krijgsman, W., F. J. Hilgen, I. Raffi, F. J. Sierro, and D. S. Wilson (1999), Chronology, causes and progression of the Messinian salinity crisis, *Nature*, *400*, 652–655, doi:10.1038/23231.

Krijgsman, W., M.-M. Blanc-Valleron, R. Flecker, F. J. Hilgen, T. J. Kouwenhoven, D. Merle, F. Orszag-Sperber, and J.-M. Rouchy (2001), The onset of the Messinian salinity crisis in the Eastern Mediterranean (Pissouri Basin, Cyprus), *Earth Planet. Sci. Lett.*, *194*(3–4), 299–310.

Kuiper, K. F., F. J. Hilgen, J. Steenbrink, and J. R. Wijbrans (2004), $^{40}Ar/^{39}Ar$ ages of tephras intercalated in astronomically tuned Neogene sedimentary sequences in the Mediterranean, *Earth Planet. Sci. Lett.*, *222*, 583–597, doi:10.1016/j.epsl.2004.03.005.

Kuiper, K. F., A. Deino, F. J. Hilgen, W. Krijgsman, P. R. Renne, and J. R. Wijbrans (2008), Synchronizing Rock Clocks of Earth History, *Science*, *320*(5875), 500–504, doi:10.1126/science.1154339.

Laepple, T., and G. Lohmann (2009), Seasonal cycle as template for climate variability on astronomical timescales, *Paleoceanography*, *24*, PA4201, doi:10.1029/2008PA001674.

Laskar, J. (1990), The chaotic motion of the solar system: A numerical estimate of the size of the chaotic zones, *Icarus*, *88*(2), 266–291, doi:10.1016/0019-1035(90)90084-M.

Laskar, J. (1999), The limits of Earth orbital calculations for geological time-scale use, *Philos. Trans. R. Soc. London A*, *357*, 1735–1759, doi:10.1098/rsta.1999.0399.

Laskar, J., P. Robutel, F. Joutel, M. Gastineau, A. Correia, and B. Levrard (2004), A long-term numerical solution for the insolation quantities of the Earth, *Astron. Astrophys.*, *428*, 261–285, doi:10.1051/0004-6361:20041335.

Laskar, J., A. Fienga, M. Gastineau, and H. Manche (2011a), La2010: A new orbital solution for the long-term motion of the Earth, *Astron. Astrophys.*, *532*, A89, doi:10.1051/0004-6361/201116836.

Laskar, J., M. Gastineau, J. B. Delisle, A. Farrés, and A. Fienga (2011b), Strong chaos induced by close encounters with Ceres and Vesta, *Astron. Astrophys.*, *532*, L4, doi:10.1051/0004-6361/201117504.

Lourens, L. J., A. Antonarakou, F. J. Hilgen, A. A. M. Van Hoof, C. Vergnaud-Grazzini, and W. J. Zachariasse (1996), Evaluation of the Plio-Pleistocene astronomical timescale, *Paleoceanography*, *11*(4), 391–413, doi:10.1029/96PA01125.

Lourens, L. J., F. J. Hilgen, J. Laskar, N. J. Shackleton, and D. Wilson (2004), The Neogene Period, in *A Geological Timescale 2004*, edited by F. Gradstein, J. Ogg, and A. Smith, pp. 409–440, Cambridge Univ. Press, Cambridge, U. K.

Lourens, L. J., A. Sluijs, D. Kroon, J. C. Zachos, E. Thomas, U. Röhl, J. Bowles, and I. Raffi (2005), Astronomical pacing of late Palaeocene to early Eocene global warming events, *Nature*, *435*(7045), 1083–1087, doi:10.1038/nature03814.

Machlus, M., S. R. Hemming, P. E. Olsen, and N. Christie-Blick (2004), Eocene calibration of geomagnetic polarity time scale reevaluated: Evidence from the Green River Formation of Wyoming, *Geology*, *32*(2), 137–140, doi:10.1130/G20091.1.

Min, K., R. Mundil, P. R. Renne, and K. R. Ludwig (2000), A test for systematic errors in $^{40}Ar/^{39}Ar$ geochronology through comparison with U/Pb analysis of a 1.1-Ga rhyolite, *Geochim. Cosmochim. Acta*, *64*(1), 73–98, doi:10.1016/S0016-7037(99)00204-5.

Murphy, B. H., K. A. Farley, and J. C. Zachos (2010), An extraterrestrial 3He-based timescale for the Paleocene-Eocene thermal maximum (PETM) from Walvis Ridge, IODP Site 1266, *Geochim. Cosmochim. Acta*, *74*(17), 5098–5108, doi:10.1016/j.gca.2010.03.039.

Ogg, J. G., and A. G. Smith (2004), The geomagnetic polarity time scale, in *A Geological Timescale 2004*, edited by F. Gradstein, J. Ogg, and A. Smith, pp. 63–86, Cambridge Univ. Press, Cambridge, U. K.

Pälike, H., and F. Hilgen (2008), Rock clock synchronization, *Nat. Geosci.*, *1*(5), 282, doi:10.1038/ngeo197.

Pälike, H., J. Laskar, and N. J. Shackleton (2004), Geologic constraints on the chaotic diffusion of the solar system, *Geology*, *32*(11), 929–932, doi:10.1130/G20750.1.

Pälike, H., J. Frazier, and J. C. Zachos (2006a), Extended orbitally forced palaeoclimatic records from the equatorial Atlantic Ceara Rise, *Quat. Sci. Rev.*, *25*(23–24), 3138–3149, doi:10.1016/j.quascirev.2006.02.011.

Pälike, H., R. D. Norris, J. O. Herrle, P. A. Wilson, H. K. Coxall, C. H. Lear, N. J. Shackleton, A. K. Tripati, and B. S. Wade (2006b), The heartbeat of the Oligocene climate system, *Science*, *314*(5807), 1894–1898, doi:10.1126/science.1133822.

Renne, P. R., A. L. Deino, R. C. Walter, B. D. Turrin, C. C. Swisher, T. A. Becker, G. H. Curtis, W. D. Sharp, and A.-R. Jaouni (1994), Intercalibration of astronomical and radioisotopic time, *Geology*, *22*(9), 783–786, doi:10.1130/0091-7613(1994)022<0783:IOAART>2.3.CO;2.

Renne, P. R., C. C. Swisher, A. L. Deino, D. B. Karner, T. L. Owens, and D. J. DePaolo (1998), Intercalibration of standards, absolute ages and uncertainties in $^{40}Ar/^{39}Ar$ dating, *Chem. Geol.*, *145*, 117–152, doi:10.1016/S0009-2541(97)00159-9.

Renne, P. R., R. Mundil, G. Balco, K. Min, and K. R. Ludwig (2010), Joint determination of 40K decay constants and $^{40}Ar^*/^{40}K$ for the Fish Canyon sanidine standard, and improved accuracy for $^{40}Ar/^{39}Ar$ geochronology, *Geochim. Cosmochim. Acta*, *74*(18), 5349–5367, doi:10.1016/j.gca.2010.06.017.

Rivera, T. A., M. Storey, C. Zeeden, F. J. Hilgen, and K. Kuiper (2011), A refined astronomically calibrated $^{40}Ar/^{39}Ar$ age for Fish Canyon sanidine, *Earth Planet. Sci. Lett.*, *311*(3–4), 420–426, doi:10.1016/j.epsl.2011.09.017.

Roger, S., P. Münch, J. J. Cornée, J. P. Saint Martin, G. Féraud, S. Pestrea, G. Conesa, and A. Ben Moussa (2000), $^{40}Ar/^{39}Ar$ dating of the pre-evaporitic Messinian marine sequences of the Melilla basin (Marocco): A proposal for some biosedimentary events as isochrons around the Alboran Sea, *Earth Planet. Sci. Lett.*, *179*, 101–113, doi:10.1016/S0012-821X(00)00094-7.

Röhl, U., and L. J. Abrams (2000), High-resolution, downhole and non-destructive core measurements from Sites 999 and 1001 in the Caribbean Sea: Application to the Late Paleocene Thermal Maximum, *Proc. Ocean Drill. Program Sci. Results*, *165*, 191–203.

Röhl, U., T. Westerhold, T. J. Bralower, and J. C. Zachos (2007), On the duration of the Paleocene-Eocene thermal maximum (PETM), *Geochem. Geophys. Geosyst.*, *8*, Q12002, doi:10.1029/2007GC001784.

Schoene, B., and S. A. Bowring (2006), U-Pb systematics of the McClure Mountain syenite: Thermochronological constraints on the age of the $^{40}Ar/^{39}Ar$ standard MMhb, *Contrib. Mineral. Petrol.*, *151*(5), 615–630, doi:10.1007/s00410-006-0077-4.

Schoene, B., J. L. Crowley, D. J. Condon, M. D. Schmitz, and S. A. Bowring (2006), Reassessing the uranium decay constants for geochronology using ID-TIMS U-Pb data, *Geochim. Cosmochim. Acta*, *70*(2), 426–445, doi:10.1016/j.gca.2005.09.007.

Schulz, M., W. H. Berger, M. Sarnthein, and P. M. Grootes (1999), Amplitude variations of 1470-year climate oscillations during the last 100,000 years linked to fluctuations of continental ice mass, *Geophys. Res. Lett.*, *26*(22), 3385–3388, doi:10.1029/1999GL006069.

Shackleton, N. J., A. Berger, and W. R. Peltier (1990), An alternative astronomical calibration of the lower Pleistocene timescale based on ODP Site 677, *Trans. R. Soc. Edinburgh Earth Sci.*, *81*, 251–261, doi:10.1017/S0263593300020782.

Shipboard Scientific Party (2004), Site 1262, *Proc. Ocean Drill. Program Initial Rep.*, *208*, 1–92.

Sierro, F. J., F. J. Hilgen, W. Krijgsman, and J. A. Flores (2001), The Abad composite (SE spain): A Messinian reference section for the Mediterranean and the APTS, *Palaeogeogr. Palaeoclimatol. Palaeoecol.*, *168*, 141–169.

Simon, J. I., P. R. Renne, and R. Mundil (2008), Implications of pre-eruptive magmatic histories of zircons for U/Pb geochronology of silicic extrusions, *Earth Planet. Sci. Lett.*, *266*, 182–194, doi:10.1016/j.epsl.2007.11.014.

Sprovieri, M., R. Coccioni, F. Lirer, N. Pelosi, and F. Lozar (2006), Orbital tuning of a lower Cretaceous composite record (Maiolica Formation, central Italy), *Paleoceanography*, *21*, PA4212, doi:10.1029/2005PA001224.

Storey, M., R. A. Duncan, and C. C. Swisher III (2007), Paleocene-Eocene Thermal Maximum and the opening of the Northeast Atlantic, *Science*, *316*(5824), 587–589, doi:10.1126/science.1135274.

Swisher, C. C., et al. (1992), Coeval $^{40}Ar/^{39}Ar$ ages of 65.0 million years ago from Chicxulub crater melt rock and Cretaceous-Tertiary boundary tektites, *Science*, *257*(5072), 954–958, doi:10.1126/science.257.5072.954.

Swisher, C. C., L. Dingus, and R. F. Butler (1993), $^{40}Ar/^{39}Ar$ dating and magnetostratigraphic correlation of the terrestrial Cretaceous-Paleogene boundary and Puercan Mammal Age, Hell Creek-Tullock formations, eastern Montana, *Can. J. Earth Sci.*, *30*(9), 1981–1996, doi:10.1139/e93-174.

Tjallingii, R., U. Röhl, M. Kölling, and T. Bickert (2007), Influence of the water content on X-ray fluorescence core-scanning measurements in soft marine sediments, *Geochem. Geophys. Geosyst.*, *8*, Q02004, doi:10.1029/2006GC001393.

van Assen, E., K. F. Kuiper, N. Barhoun, W. Krijgsman, and F. J. Sierro (2006), Messinian astrochronology of the Melilla Basin: Stepwise restriction of the Mediterranean–Atlantic connection through Morocco, *Palaeogeogr. Palaeoclimatol. Palaeoecol.*, *238*(1–4), 15–31, doi:10.1016/j.palaeo.2006.03.014.

Westerhold, T., and U. Röhl (2006), Data report: Revised composite depth records for Shatsky Rise Sites 1209, 1210, and 1211, *Proc. Ocean Drill. Program Sci. Results*, *198*, 1–26.

Westerhold, T., and U. Röhl (2009), High resolution cyclostratigraphy of the early Eocene–New insights into the origin of the Cenozoic cooling trend, *Clim. Past*, *5*(3), 309–327, doi:10.5194/cp-5-309-2009.

Westerhold, T., U. Röhl, J. Laskar, J. Bowles, I. Raffi, L. J. Lourens, and J. C. Zachos (2007), On the duration of magnetochrons C24r and C25n and the timing of early Eocene global warming events: Implications from the Ocean Drilling Program Leg 208 Walvis Ridge depth transect, *Paleoceanography*, *22*, PA2201, doi:10.1029/2006PA001322.

Westerhold, T., U. Röhl, I. Raffi, E. Fornaciari, S. Monechi, V. Reale, J. Bowles, and H. F. Evans (2008), Astronomical calibration of the Paleocene time, *Palaeogeogr. Palaeoclimatol. Palaeoecol.*, *257*(4), 377–403, doi:10.1016/j.palaeo.2007.09.016.

Westerhold, T., U. Röhl, H. K. McCarren, and J. C. Zachos (2009), Latest on the absolute age of the Paleocene-Eocene Thermal Maximum (PETM): New insights from exact stratigraphic position of key ash layers +19 and −17, *Earth Planet. Sci. Lett.*, *287*(3–4), 412–419, doi:10.1016/j.epsl.2009.08.027.

Westerhold, T., U. Röhl, B. Donner, H. K. McCarren, and J. C. Zachos (2011), A complete high-resolution Paleocene benthic stable isotope record for the central Pacific (ODP Site 1209), *Paleoceanography*, *26*, PA2216, doi:10.1029/2010PA002092.

Wilson, D. S. (1993), Confirmation of the astronomical calibration of the magnetic polarity timescale from sea-floor spreading rates, *Nature*, *364*, 788–790, doi:10.1038/364788a0.

Zachos, J., N. J. Shackleton, J. S. Revenaugh, H. Pälike, and B. P. Flower (2001), Climate response to orbital forcing across the Oligocene-Miocene boundary, *Science*, *292*, 274–278, doi:10.1126/science.1058288.

Zachos, J. C., et al. (2004), *Proceedings of the Ocean Drilling Program, Initial Reports*, vol. 208, Ocean Drill. Program, College Station, Tex.

Zachos, J. C., H. McCarren, B. Murphy, U. Röhl, and T. Westerhold (2010), Tempo and scale of late Paleocene and early Eocene carbon isotope cycles: Implications for the origin of hyperthermals, *Earth Planet. Sci. Lett.*, *299*(1–2), 242–249, doi:10.1016/j.epsl.2010.09.004.